An Interface Design for Axial Induction Motor

Erkan Er[1], Mehmet Tahir Güllüoğlu[2]

[1] Vocational School of Viranşehir, Harran University, Şanlıurfa, Turkey
[2] Department of Electrical and Electronics Engineering, Harran University, Şanlıurfa, Turkey
Corresponding Author : mtahir@harran.edu.tr

ABSTRACT

Asynchronous motors have been used extensively in the industry since the first discovery. Although the general working principles do not change, they can be made geometrically in the form of cylinders, spheres, cones and even discs. One of these geometries is known as axial flux machine topology which has a disc structure. Axial flux machines are remarkable in terms of their high efficiency, high power density and advantage in terms of compact structures. In this study, extended literature search of axial flux induction motor is given. In addition to the literature, axial induction motor design interface has been created by using MATLAB GUI software. This interface can communicate with ANSYS Maxwell. Thus, the dimensioning values of the machine calculated via the interface can be drawn automatically in Ansys Maxwell and it can perform numerical analysis. The obtained torque, current and efficiency data were evaluated.

1. INTRODUCTION.

Induction motors; single excitation, simple structure, acceptable yields are preferred because they can be produced at low cost. Although the asynchronous motor is spread as a conventional structure (radial flux), it can be designed as disc type (axial flux). The axial flux induction motor (AFIM) is very similar to the asynchronous motor in the traditional structure and the materials used in the structure. The first electric machine using the axial flux system with the principle of electromagnetic induction is the primitive disc machine introduced by Faraday in 1821. In later years, the radial flux machine became popular and popular. However, in recent years there have been patents on different structures of AFIM (Varga, 1990; Kliman *et al*., 2002; Carl and Stephens, 2004; Pyrhonen and Piispanen. 2008). By comparing the AFIM torus type motor with conventional asynchronous motor, torque density is shown to be 2.62 times higher than AFIM (Sakai et al., 2018). Although AFIM is the same diameter as conventional asynchronous motor, it is stated that AFIM is more compact. Again, the equivalent circuit parameter analysis result for Torus type AFIM was compared with the numerical analysis result obtained by two-three-dimensional finite element method (Nobahari *et al.,* 2017). In the equivalent circuit parameter results, the % 3 - 8% error is due to the fact that the winding final inductance value is not included in the calculation. Another remarkable study in the literature is the example of the effect of the use of superconducting material on the power capacity, the internal diameter of the motor (Di / Do) ratio and the pole number to reduce winding losses (Gonzalez-Parada et al., 2012). In the first of their two studies on squirrel cage AFIM, an experimental test and analytical study of a squirrel cage, high -

efficiency, single-stator single rotor axial flux induction machine prototype made of copper was made based on the results and analytical calculations (Tapia et al., 2016; 2017). In their other studies, a single stator, single rotor axial flux induction prototype was evaluated analytically and numerically with a squirrel cage made of copper by calculating the Carter factor to estimate the magnetizing current required for the motor in different air gap lengths. In an axial flux induction machine, the diagnostic properties of axial flux as a result of asymmetry of electrical and magnetic circuits have been investigated (Jarzyna, 1995). Analytical explanation of the theoretical basis of the current layer theory of squirrel-cage single stator AFIM, flux density in the air gap, ringing flux of the stator and rotor, electromagnetic torque, and parameters of a phase equivalent circuit have been made (Igelspacher and Herzog, 2010). Two-phase axial flux disc rotor induction motor applications are presented with experience (Dwivedi *et al*., 2015).

The axial flux induction motor can also be used in the automobile drive system because of the power density advantages of the disc motor (Mushid and Dorrell, 2017). For example, there are studies on single stator for electric vehicles - design and application of single rotor AFIM (Ashari et al., 2014), differential use of double rotor AFIM in electric vehicles (Neelima *et al*., 2014), driver circuits for AFIM used for electric cars (Profumo *et al*., 1997), studies on the single-phase simulation of axial flux induction machines (Smith and Platt, 1990) in the double rotor single stator AFIM for driving the two wheels of an electric vehicle. The design and performance analysis of a new motor driver was carried out for two AFIMs where a rotating part of each engine was mounted to the wheel rim and the fixed part was mounted to the chassis structure

of an experimental electric vehicle (Benoudjit et al., 2000).

A new method, which is known as stator discharge current, is used to estimate the electrical parameters of the single-phase axial flux induction motor (Nasiri-Gheidari and Lesani, 2012b). By taking into account saturation, anisotropy and harmonics and by using imperialist competition algorithm, it is provided to optimize the total harmonic distortion of the air gap flux density in order to minimize torque vibration in single-phase axial flux induction motors (Nasiri-Gheidari and Lesani, 2012c). The torque-velocity characteristic of a single-phase capacitor-operated cage AFIM was investigated using two-dimensional finite element method (2D SEY) and theoretical method (Nasiri-Gheidari and Lesani, 2014). In their other studies, they studied axial induction motor design using 3D SEY and dq mathematical method (Nasiri-Gheidari and Lesani, 2013c). For direct drive operation, a new optimized structure for a two-speed, condenser, single-phase axial flux induction motor with adjustable air gap is introduced (Nasiri-Ghedari and Lesani, 2013b). Performance estimation was performed by considering the effect of core saturation, supply voltage and eccentricity of a single phase capacitor operating under static eccentricity, and examining the transient and permanent mathematical model based on the d-q axis theory (Nasiri-Gheidari *et al.*, 2014). Nasiri-Zarandi and Mirsalim (2015) discussed the analysis and torque calculation of an axial flux hysteresis motor. A new approach for the design and construction of axial flux induction motors with medium-power anisotropic rotor is presented (Wallace *et al.*, 1991). Analytical modeling was performed using a three-dimensional method to help designers calculate and evaluate the performance of mass rotor axial air gap induction machines in a shorter period of time (Mirzaei *et al.*, 2007). A rotating magnetic field model of AFIM has been developed for the geometric properties of the stator and rotor core, and the main geometric dimensions of the different types of induction motors have been compared using field model formulas (Varga, 1986).

A new AFIM with three wells and three coils has been proposed for the elevation system (Shuo *et al.*, 2011). The experience of time harmonic three-dimensional (3D) finite element analysis applications in the analysis of axial flux mass rotor asynchronous motor is discussed (Valtonen et al., 2006). The length of the air gap between the stator and the rotor is known to affect engine performance. They examined the effect of the air gap length between rotor and stator in the disc motor on motor performance (losses, slip, efficiency, etc.) (Valtonen et al., 2008). The effects of the number of rotor grooves of the axial flux mass rotor core induction motor on the performance, electromagnetic torque generation, torque fluctuation, rotor losses and the power factor of the motor have been demonstrated (Valtonen *et al.*, 2007a). In another study, the effect of switching frequency of an inverter on the performance of rotor losses of an axial flux mass rotor core induction motor was investigated (Valtonen *et al.,* 2007b).

There are many methods for increasing the efficiency of the asynchronous motor. These methods; open slits in rotor and stator (Arslan at al., 2017) increase the amount of active substance, use longer package length, use double layer windings, use high quality and lower loss lamination materials (Arslan, 2016), rotor use of better quality aluminum material or copper for the surface, improve fan assembly efficiency, improve rotor design, and optimize the air gap between the stator and rotor (Gök, 2015). Increasing the air gap increases the magnetization current, which leads to an increase in iron losses and a decrease in the power factor (Çunkaş, 2012). There are many studies examining the change of some design parameters or core material of induction motor using RMxprt and

Maxwell (Ping et al., 1999; Tarimer, 2005; Deshmukh *et al.*, 2014).

2. STRUCTURE OF AXIAL FLUX INDUCTION MOTOR

Axial flux induction motors are a motor structure in which the windings producing the magnetic field are positioned radially and the generated magnetic field occurs parallel to the axis of rotation of the motor. Induction motors of conventional structure are defined as radial motors. In these motors, windings are motors in which the motor is placed parallel to the axis of rotation and the magnetic flux occurs radially.

The axial flux motors have a ring structure in the stator, while the rotor cores are in disk structure. In conventional motors with radial flux, the main dimensions are core diameter and length, while in axial flux motors, the main dimensions are the inner diameter and the outer diameter length of the core. Since the axial flux machine has a larger diameter-to-length ratio and the internal diameter will generally be larger than the shaft diameter, much better ventilation and cooling can be achieved than conventional motors. Higher specific electrical loading and possible use of higher specific magnetic loads will further reduce the size of the axial flux machines (Nasiri-Ghedari and Lesani, 2012a). When the radial flux motor with the same diameter and core length is compared with the axial flux motor, the axial flux motor has been found to be twice as high in terms of maximum torque and torque density (Sakai et al., 2018). The different configurations of the standing part stator and the rotating part rotor that produce the magnetic field in the structure of the AFIMs have provided three different types of motors; single air space, double air space, multi air space engine. The single sided axial-flux induction motor is given in Figure 1.
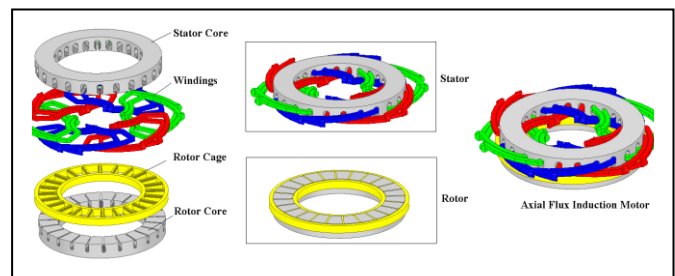

Figure 1. Single sided axial-flux induction motor

3. SIZING EQUATIONS OF SINGLE SIDED AXIAL-FLUX INDUCTION MOTOR

The most basic mechanical data for motor power in axial flux induction motors is the inner diameter (Di) and the outer diameter (Do). The ratio of inner diameter to outer diameter is given in Equation (1) with an expression such as kd.

$$k_d = \frac{D_i}{D_o} \qquad (1)$$

The outer radius (Rout) and the inner radius (Rin) are used to calculate the core length (le) of the motor. The outer radius, inner radius and core length are specified in Equation (2), (3) and (4), respectively.

$$R_{out} = 0.5D_o \qquad (2)$$

$$R_{in} = 0.5D_i \qquad (3)$$

$$l_e = R_{out} - R_{in} \qquad (4)$$

The mean radius value of the motor (Ravg) and the power and torque generating surface area (Sr) expressions connected to the inner radius and the outer radius are also shown in Equations (5) and (6), respectively.

$$D_{avg} = \sqrt{D_{out} D_{in}} \tag{5}$$

$$S_r = \pi (R_{out}^2 - R_{in}^2) \tag{6}$$

The magnetic charge is the maximum flux density produced by the core to produce the rotational force (B). The flux density affects the amount of magnetic flux produced by the core. Simply put, the amount of flux is the product of flux-producing area and flux density. Equation of the amount of magnetic flux is given in Equation (7).

$$\emptyset = \oint B dA \tag{7}$$

The flux density (Bds) in the stator core is calculated using Equation (8) for each diameter case using the distance between the stator grooves (τs), the groove width (bs), and the flux density (Bδ) in the air gap.

$$B_{ds(1...n)} = \frac{B_\delta \tau_{s(1...n)}}{\tau_{s(1...n)} - b_s} \tag{8}$$

When determining the number of stator grooves, the number of phases of the motor and the number of poles are taken into account. The multiplication of the two allows us to find the number of stator grooves. The core surface area (Sp) per pole according to the number of poles of the motor (p) is found by Equation (9).

$$S_p = \frac{S_r}{p} \tag{9}$$

Let us first express the winding factors in the design of the stator windings. In induction motors, step shortening, and winding distribution methods are applied in order to eliminate the harmonics that may occur in the voltages induced in the windings. These methods are called distribution coefficient (Kb) and step coefficient (Kp) in the calculation of winding number. A single winding factor (Kw) is shown in the equation. Winding factor, distribution coefficient and step coefficient equations are given in Equation (10), (11) and (12) respectively.

$$K_w = K_b K_p \tag{10}$$

$$K_b = \frac{\sin(C\frac{\alpha}{2})}{C\sin(\frac{\alpha}{2})} \tag{11}$$

$$K_p = \cos(\frac{\beta}{2}) \tag{12}$$

Part of the phase voltage applied to the stator will decrease in stator impedance. The remaining voltage is the voltage induced in the windings (Es) and is 97% of the phase voltage (Boldea and Nasar, 2002). Starting from the emk formula of induction motors, the winding number of the stator winding (Ns) is found by Equation (13).

$$N_s = \frac{E_s}{4,44 f \emptyset K_w} \tag{13}$$

The amount of current to pass through the windings (Is) can be obtained from the three-phase general power equation. If the output power of the stator windings of the star connected motor is known, the current drawn from the source can be found using Equation (14).

$$I_s = \frac{P_\varsigma}{\sqrt{3}V \cos\varphi\eta} \tag{14}$$

The power expression of the motor is the mechanical data and the torque multiplied by the angular rotor speed. Equation (15) obtained by the synchronous is angular velocity (ws). The estimated angular velocity (wr) of the rotor for 6% shear value is given in Equation (15) and the power and torque relative to the angular velocity are given in Equation (16).

$$w_r = w_s - (S.w_s) \tag{15}$$

$$T = \frac{P}{w_r} \tag{16}$$

Since torque is a rotational force proportional to the shaft axis, torque is the product of the tangential force (Fσtan), the rotor average radius (Ravg) and the surface area (Sr). Equation (17) and the torque statement are written. Equation (18) is obtained by pulling the tangential force from this equation.

$$T = S_r R_{avg} F_{\sigma tan} \tag{17}$$

$$F_{\sigma tan} = \frac{T}{S_r R_{avg}} \tag{18}$$

Equation (19) is obtained with the data of magnetic flux density (B) and total current density (j) of the conductors.

$$F_{\sigma tan} = \frac{B.j}{2} \tag{19}$$

The total conductor current density can be obtained by the total number of conductors (Z) and the average stator diameter (D) of the three phases. Equations of total number of conductors, mean diameter and total current density are given in Equations (20), (21) and (22), respectively.

$$Z = 2.m.N \tag{20}$$

$$D = 2R_{avg} \tag{21}$$

$$A = \frac{I.Z}{\pi.D} \tag{22}$$

In the rotor design, the flux density in the core is calculated exactly as in the stator. The equation (8) is shown in Equation (23) for the rotor magnetic flux.

$$B_{dr(1...n)} = \frac{B_\delta \tau_{r(1...n)}}{\tau_{r(1...n)} - b_r} \tag{23}$$

The distance of the air gap (Lag) between the rotor and the stator is very effective in rotor performance. Experimentally (Ashari et al., 2014) the distance of the optimum air gap can be calculated by the equation given in Equation (24).

$$L_{ag} = 3,06 - \frac{6560}{D + 2280} \tag{24}$$

4. DESIGNED INTERFACE

ABAQUS, ANSYS (MAXWELL), COMSOL, FEMLAB, FLUX 2D/3D and INFOLYTICA (MAGNET, ELECNET, etc.) are used to solve electrical, magnetic and engineering problems. These software programs perform numerical analysis using finite element method. Some of these programs have ready-made design interfaces and can even perform numerical analysis of the machine geometry discussed (Arslan, 2016). There are many studies examining the

change of some design parameters or core material of induction motor using RMxprt and Maxwell (Ping et al., 1999; Tarimer, 2005; Çunkaş, 2012; Deshmukh et al., 2014; Gök, 2015). In addition, general literature research study on AFIM was conducted in detail by Nasiri-Gheidari and Lesani (2012a). Unlike other studies in the literature (Arslan et al., 2019; Arslan et al., 2018; Arslan et al., 2019), the design interface for the axial machine is created in Matlab-GUI. However, Ansys Maxwell has the module Rmxprt for the analytical solution of rotary machines. This module performs analytical analysis of rotary machines. As it is known, although the analytical equations used for the design of electrical machines can achieve fast results, it is insufficient to fully examine the working condition of the machine. Although it is more accurate to perform with finite element analysis, the analysis takes longer time. This interface has been designed to take advantage of the analytical and numerical approach for the axial flux machine.

Ansys Maxwell, which can work dynamically with Visual Basic Script and Python languages, has been chosen as the finite element software program (Arslan et al., 2019). The Visual Basic code of the basic model created in Ansys Maxwell is defined in Matlab Gui. In addition, the basic geometry data of the machine is obtained through analytical sizing equations defined in Matlab Gui. An analysis of the axial machine can be performed according to the sizing data obtained from Ansys Maxwell different processing tools (Transient, Optimization, etc.) defined in Matlab Gui. For Ansys Maxwell and Matlab Gui communication, code conversions and mathematical formulas must be defined in the interface. The model, which is transformed into Matlab code, is a dynamic structure and the change of the design sizing parameters allows the optimization of the design model. Thus, the package manufacturers make the package programs dynamic instead of creating a ready interface for each machine topology. In short, the solution and design of different machines can be realized by using open software code of package programs. The code transformation flowchart discussed in this study is shown in Figure 2:
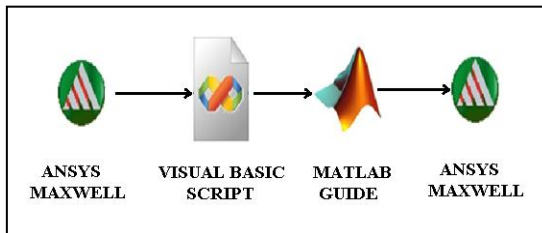

Figure 2. Interface analytical and numerical analysis process

In Ansys-Maxwell settings, the communication protocol of the two programs is established by showing the address of the .exe file of the Matlab program. Axial flux model geometry is saved in Ansys-Maxwell Script file. In this study, the code recorded as .vbs has been converted to Matlab code. In Matlab Gui, the code is entered under pushbutton as it is provided with pushbutton for performing analytical calculations. Separate definition should be made for the solver module (transient, electrostatic, eddy current, etc.) in which the design problem discussed should work. In this study, only the transient state is discussed. The designed interface is shown in Figure 3 below.
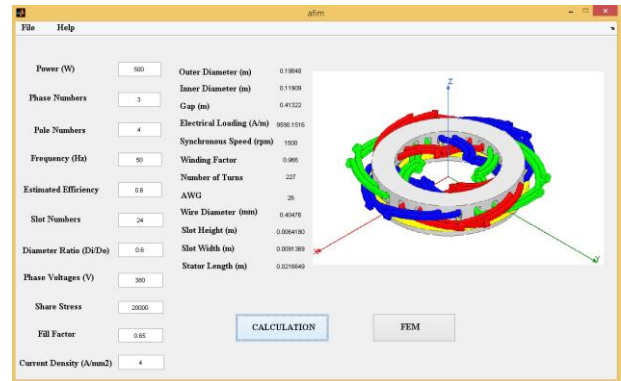

Figure 3. Interface view

5. THE ANSYS MAXWELL MODEL AND NUMERICAL SIMULATION

In order to examine the design of the asynchronous motor, the model created in ANSYS RMXprt was modeled in ANSYS Maxwell 3D environment and design and analysis studies were performed. ANSYS Maxwell 3D module transient analysis module was used since this module could not be transformed due to axial geometry for model 2D transient analysis designed in ANSYS RMXprt module. For transient analysis models, analysis time was 0.1 sec and analysis step was selected as 0.2 msec. Analysis of the acceleration and torque values of the analyzed models were performed. Ansys Maxwell 3D model, which was created considering Figure 3, is given in Figure 4.
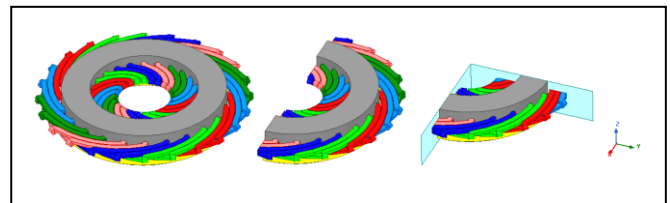

Figure 4. Making the model 1/4 for the model solution

Here, it is divided into 4 parts due to the motor pole to accelerate the solution for the 3-dimensional geometry of the model. Similarly, for different pole combinations, model 1/2, 1/4, 1/8 and so on. can be divided into parts. Axis symmetries can be applied to different machine models. In Ansys Maxwell, Master, Slave definitions are made, and the model is solved. As already mentioned, the definitions to be performed for motor analysis can be determined as excitation, the desired quantities to be calculated can be determined as force, torque. In order to perform full load analysis in the moving part; if (speed <128.822, -0.0301295 * speed, -500 / speed). External circuit model is used for the voltage applied to the motor. The motor phase windings are connected to the star and applied voltage is different from 120-degree phase, voltage and current probes are identified and analyzed. Full load analysis Analyzes were performed on a computer with i7-6700 3.4 GHz processor and 16 GB ram. The transient time analysis lasted 30 hours and 13 minutes.
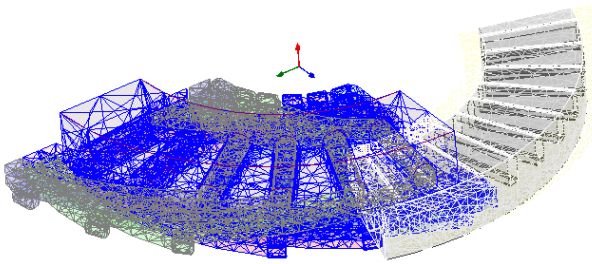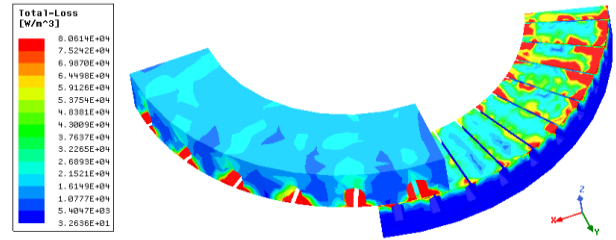
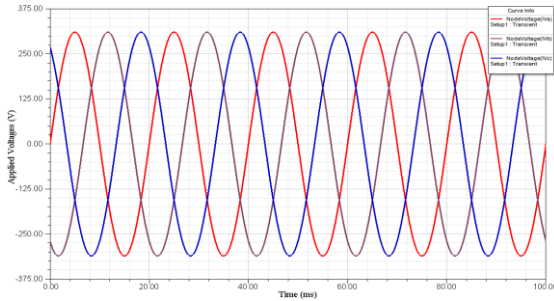**Figure 5.** Mesh structure of the model

Figure 6. Change of applied voltage

Figure 7. Change of phase currents

Figure 8. Induced voltage changes in phase windings

The number of mesh assigned to the model is 69758. The mesh structure of the model is shown in Figure 5, the waveform of the applied voltage is shown in Figure 6, the waveform of the phase currents is shown in Figure 7 and the waveform of the induced voltage in the phase windings is shown in Figure 8.

When the curves are examined, the voltage applied to the windings is a three-phase voltage different from 120° phase with a peak value of 311 V. After 60 ms, continuous operating values are read out. The peak value is approx. 3 A with phase currents and the 300 V induced winding is read. It is determined as M19-29G because it has very low losses in non-oriented sheet metal which is considered to be used in stator and rotor. Iron losses have increased in areas where flux density has increased. Especially in rotor and stator teeth this change is shown in Figure 9.

Figure 9. Change in iron loss intensity

Figure 9 examined the total iron loss in the stator and rotor was found to be 6.6 W. When Figure 10 is examined, the current passing through the phase windings increases at the first time and creates a similar change in copper loss.
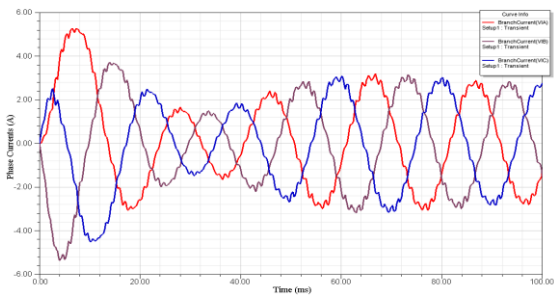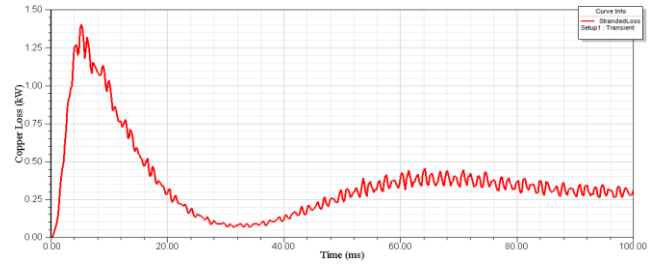

Figure 10. Change of copper loss

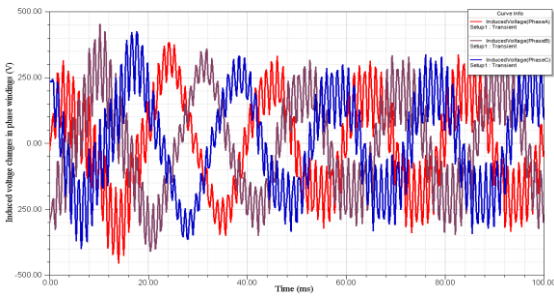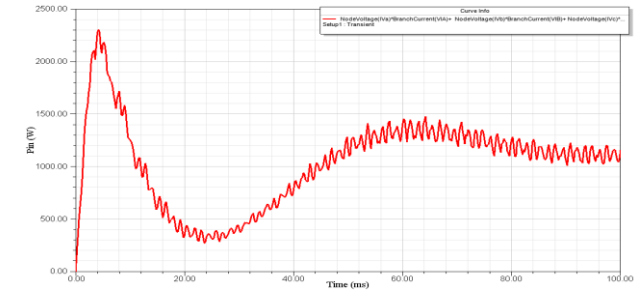The input power and output power variation of the motor is shown in Figure 11 and Figure 12, respectively.

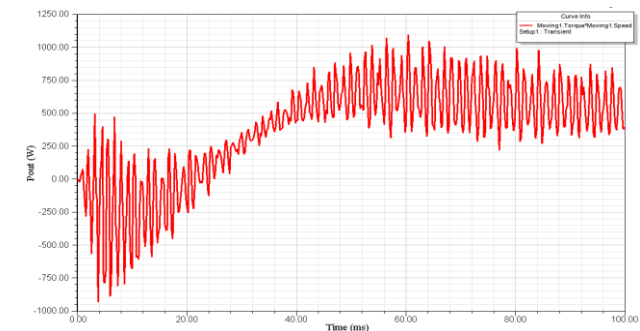
Figure 11. Change of input power

Figure 12. Change of output power

When the curves were examined, the continuous input power was calculated as 1116.27 W and the output power was 592 W. The flux density change in the rotor and stator at 90 ms is shown in Figure 13.
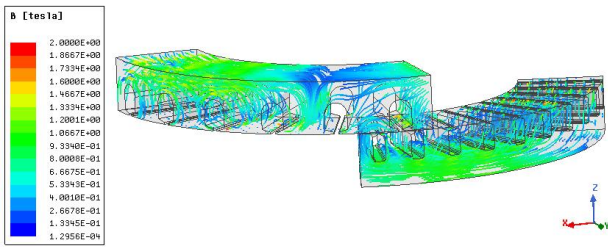
Figure 13. Magnetic flux density changes of rotor and stator

Maximum magnetic flux densities can be limited to stator yoke 1.7 T, stator tooth 2.1 T, rotor yoke 1.7 T, rotor tooth 2.2 T respectively (Lipo, 2004). Working in areas close to these values may affect engine dimensions and motor thermal values. Since the flux density in the rotor and stator yoke is less than 2 T, the sheet material is not expected to reach saturation. In addition, the flux density in the stator yoke is maximum 1.6 T, and the rotor yoke flux density is 1.3 T. Figure 14 gives the current density in the phase windings.
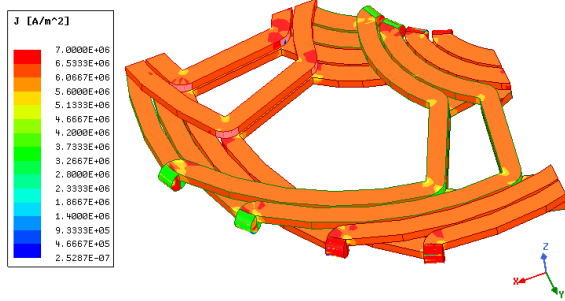

Figure 14. Change of stator current density

Here the current density change is seen as about 5.5 A/mm^2. The effect of the inclination in the rotor grooves of the loaded motor on electromagnetic torque was investigated by parametric analysis. Starting from 0 degrees to 10 degrees, electromagnetic torque change was investigated by changing step by step 2.5 degrees. The inclination of the rotor bars is shown in Figure 15, the result of electromagnetic torque change is shown in Figure 16.
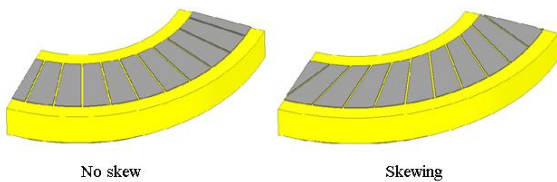

Figure 15. Straight and curved shapes of rotor grooves

Here, the increase in the inclination of the rotor rod with the change of electromagnetic torque peak to peak value, iron losses change is shown in Table 1.

Table 1. Electromagnetic torque changes according to the angle of inclination

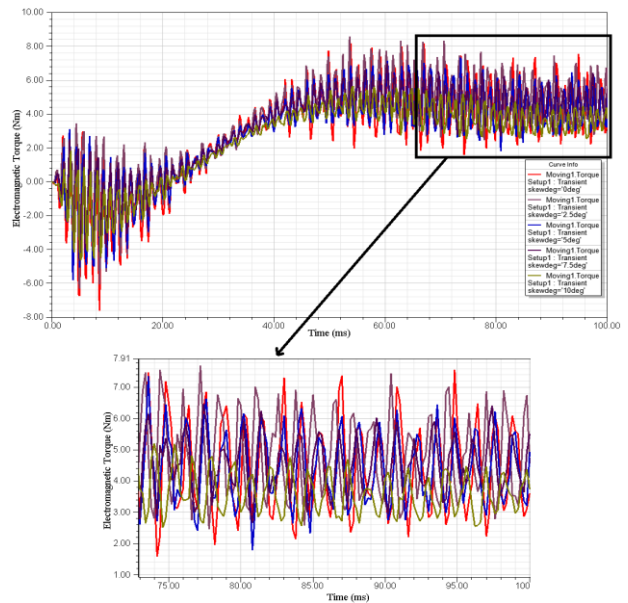| Skew Angle (Degrees)	Peak to Peak Torque (Nm)	Torque (Nm)	Iron loss (W)
0	5.39	4.5	6.68
2.5	4.84	4.9	6.69
5	4.63	4.43	6.97
7.5	3.74	4.63	7.52
10	2.19	3.58	7.95

Figure 16. Change of electromagnetic torque by inclination of rotor rods

According to the results given in Table 4.1, as the inclination increases, the torque amount produced by the motor decreases despite the torque ripple improvement. In addition, there was no change in copper losses. However, the change in iron losses increases with increasing slope.

Three dimensional transient state analyzes of axial flux motor were performed. Prototype production can be realized by performing optimization studies on the obtained sizing data. Considering that a single analysis of the model reduced to 1/4 takes approximately one day, it is time-consuming to make calculations using supercomputer or parallel connected computers for optimization studies. However, it should be noted that the use of two methods may be costly to the user.

6. CONCLUSION

In this study, the motor interface has been developed in line with the basic analytical sizing equations of the axial machine. With this interface, general dimensioning of the motor is made, and the working state of the motor can be examined with finite element analysis. In this context, the outcomes obtained by the study are as follows:

- It sets an example for researchers working on axial flux machines in terms of using analytical and finite element analysis together.
- It can also be used as a training tool for training applications, especially on the design of electrical machines.
- The interface tool can perform analytical and numerical (FEM) analysis as well as optimization or different solution methods.

REFERENCES

Ashari, M., Suryoatmojo, H., Riawan, D. C., Mardiyanto, R., Fahmi, D., Hidayat, S., & Adam, K. B. (2015). Design and Implementation of Axial Flux Induction Motor Single Stator-Single Rotor for Electric Vehicle Application. *IPTEK Journal of Proceedings Series*, 1(1).

Arslan, S.., Oy, S. A., & Tarımer, I. (2017). Investigation of stator and rotor slits' effects to the torque and efficiency of an induction motor. TEM Journal, 6(1), 117.

Arslan, S., Gürdal O, Akkaya Oy S. (2019) Communication of Matlab   Gui

and Ansys Maxwell: An Education Tool For Tubular Linear Generator.*J. Fundam. Appl. Sci.*, 11(1), 117-141

Arslan, S., Gurdal, O. (2019). Polygonal Tubular Linear Permanent Magnet Generator Analysis and Experimental Test. *Scientia Iranica*, (), -. doi: 10.24200/sci.2019.50094.2739

Arslan, S. (2016). Performance Comparison of Submersible Motor Based on Numerical and Analytical Results. Duzce University Journal of Science and Technology, 4(2).

Arslan, S., Gurdal, O., Akkaya Oy, S. (2018). Design and Optimization of Tubular Linear Permanent Magnet Generator with Performance Improvement Using Response Surface Methodology and Multi-Objective Genetic Algorithm. Scientia Iranica, (), -. doi: 10.24200/sci.2018.50093.1506

Benoudjit, A. Guettafi, N. Nait Saïd, A. (2000). Axial flux induction motor for on-wheel drive propulsion system. *Electric Machines &Power Systems*, 28(12), 1107-1125.

Boldea, I. And Nasar, S.A., (2002). The Induction Machine Handbook. CRC Press LLC, USA, 946s.

Carl, J. R. And Stephens, S.M., (2004). Axial Flux Induction Motor. Patent Application Publication. USA.

Çunkaş, M., (2012). A Review on Submersible Motors. *J. Fac.Eng.Arch. Selcuk Univ.* 27(4): 136-147.

Dwivedi, A., Gupta, S. K., Singh, S. K., & Srivastava, R. K. (2015, November). Experiences with axial flux sheet rotor induction motor. In 2015 *IEEE IAS Joint Industrial and Commercial Power Systems/Petroleum and Chemical Industry Conference (ICPSPCIC)* (pp. 115-118). IEEE.

Deshmukh, A., Bhole, A. A., (2014). Optimized Design of Submersible Induction Motor Using Maxwell 16.0 Rmxprt, *IAEME*, 5(9): 39-44.

González-Parada, A., Guía, M., Ibarra, O., & Guzmán, R. (2012). Development of axial flux HTS induction motors. *Procedia Engineering*, 35, 4-13.

Gök, O., (2015). *Performance Analysis of Standard and High Efficiency Squirrel Cage Induction Motors* (Master Thesis, Dumlupınar University).

Igelspacher, J., & Herzog, H. G. (2010, September). Analytical description of a single-stator axial-flux induction machine with squirrel cage. *In the XIX International Conference on Electrical Machines-ICEM 2010* (pp. 1-6). IEEE.

Jarzyna, W., 1995. Diagnostic Characteristics of Axial Flux in An Induction Machine. *1995 Seventh International Conference on Electrical Machines and Drives (Conf. Publ. No. 412)*, 11-13 September, Durham, UK, 141-146.

K Kliman, G. B., Stephens, C. M., & Jansen, P. L. (2002). U.S. Patent No. 6,445,105. Washington, DC: U.S. Patent and Trademark Office.

Mirzaei, M., Mirsalim, M., & Abdollahi, S. E. (2007). Analytical modeling of axial air gap solid rotor induction machines using a quasi-three-dimensional method. *IEEE Transactions on Magnetics*, 43(7), 3237-3242.

Mushid, F. C., & Dorrell, D. G. (2017, April). Review of axial flux induction motor for automotive applications. *In 2017 IEEE Workshop on Electrical Machines Design, Control and Diagnosis (WEMDCD)* (pp. 146-151). IEEE.

Nasiri-Gheidari, Z., & Lesani, H. (2012). A survey on axial flux induction motors. *Przeglad Elektrotechniczny*, 2, 300-305.

Nasiri-Gheidari, Z., & Lesani, H. (2012). Using stator discharge current for the parameter estimation of a single-phase axial flux induction motor. *Scientia Iranica*, 19(6), 1794-1801.

Nasiri-Gheidari, Z., & Lesani, H. (2012). Design optimization of a single-phase axial flux induction motor with low torque ripple. *Przegląd Elektrotechniczny*, 88(3b), 168-172.

Nasiri-Gheidari, Z., & Lesani, H. (2013). Optimal design of adjustable air-gap, two-speed, capacitor-run, single-phase axial flux induction motors. *IEEE Transactions on energy conversion*, 28(3), 543-552.

Nasiri-Gheidari, Z., & Lesani, H. (2013). Investigation of characteristics of a single-phase axial flux induction motor using three-dimensional finite element method and d− q model. *IET Electric Power Applications*, 7(1), 47-57.

Nasiri-Gheidari, Z., & Lesani, H. (2014). Theoretical modeling of axial flux squirrel cage induction motor considering both saturation and anisotropy. *International Transactions on Electrical Energy Systems*, 24(3), 335-346.

Nasiri-Gheidari, Z., Lesani, H., & Tootoonchian, F. (2014). Performance prediction of a single-phase capacitor-run axial flux induction motor under static eccentricity. *Australian Journal of Electrical and Electronics Engineering*, 11(1), 93-104.

Nasiri-Zarandi, R., & Mirsalim, M. (2015). Analysis and torque calculation of an axial flux hysteresis motor based on hyperbolic model of hysteresis loop in Cartesian coordinates. *IEEE Transactions on Magnetics*, 51(7), 1-10.

Neelima, P., Manjeera, M. C., & Babu, M. V. R. (2014). Modelling of Axial Flux Induction Machines and it Application as Differential in Electrical Vehicles. *International Journal of Innovative Research in Advanced Engineering* (IJIRAE), 1(12): 1-10.

Nobahari, A., Darabi, A., & Hassannia, A. (2017, February). Axial flux induction motor, design and evaluation of steady state modeling using equivalent circuit. *In 2017 8th Power Electronics, Drive Systems & Technologies Conference (PEDSTC)* (pp. 353-358). IEEE.

Zhou, P., Stanton, S., & Cendes, Z. J. (1999, May). Dynamic modeling of three phase and single-phase induction motors. *In IEEE International Electric Machines and Drives Conference. IEMDC'99. Proceedings* (Cat. No. 99EX272) (pp. 556-558). IEEE.

Profumo, F., Zhang, Z., & Tenconi, A. (1997). Axial flux machines drives: A new viable solution for electric cars. *IEEE Transactions on Industrial Electronics*, 44(1), 39-45.

Pyrhonen, J. And Piispanen, A., (2008). Axial Flux Induction Electric Machine. Patent Application Publication. USA.

Sakai, R., Yoshida, Y., & Tajima, K. (2018). Study on Analysis of Torque-Slip Characteristics of Axial Gap Induction Motor. *Transaction of the Magnetics Society of Japan Special Issues*, 2(1), 43-47.

Shuo, L., Yu, F., Xi, Z., & Wei, Q. (2011, August). New structure of axial flux induction motor and characterization analysis. *In 2011 International Conference on Electrical Machines and Systems* (pp. 1-5). IEEE. SMITH, B. H. and PLATT, D., 1990. Compound, Series, Axial Flux İnduction Machines: Single Phase Analogy. IEE Proceedings B - Electric Power Applications, 137(4): 265-272.

Tapia, M. A., Hoffer, A. E., & Tapia, J. A. (2016, October). Analysis of the magnetizing current requirement of an axial flux induction machine. *In 2016 IEEE International Conference on Automatica (ICA-ACCA)* (pp. 1-6). IEEE.

Montero, M. A. T., Garces, A. E. H., Ladino, J. A. T., & Collao, R. R. W. (2017). Simulation and Analysis of an Axial Flux Induction Machine. *IEEE Latin America Transactions*, 15(7), 1263-1269.

Tarimer, I., (2005). Computer Aided Design of Induction Motor. Jounal of Polytechnic, 8(1): 19-24.

Valtonen, M. S. M., Parviainen, D. S. A., & PyrhOnen, J. (2006, May). Electromagnetic field analysis of 3D structure of axial-flux solid-rotor induction motor. *In International Symposium on Power Electronics, Electrical Drives, Automation and Motion, 2006. SPEEDAM 2006.* (pp. 174-178). IEEE.

Valtonen, M., Parviainen, A., & PyrhOnen, J. (2007, May). The effects of the number of rotor slots on the performance characteristics of axial-flux aluminum-cage solid-rotor core induction motor. *In 2007 IEEE*

International Electric Machines & Drives Conference (Vol. 1, pp. 668-672). IEEE.

Valtonen, M., Parviainen, A., & PyrhOnen, J. (2007, April). Inverter switching frequency effects on the rotor losses of an axial-flux solid-rotor core induction motor. *In 2007 International Conference on Power Engineering, Energy and Electrical Drives* (pp. 476-480). IEEE.

Valtonen, M., Parviainen, A., & Pyrhonen, J. (2008, September). Influence of the air-gap length to the performance of an axial-flux induction motor. *In 2008 18th International Conference on Electrical Machines* (pp. 1-5). IEEE.

Varga, J. S. (1986). Magnetic and dimensional properties of axial induction motors. *IEEE transactions on energy conversion*, (2), 137-144.

Varga, J. S., (1990). Dual Rotor Axial Air Gap Induction Motor. Patent Application Publication. USA.

Wallace, R., Moran, L., Cea, G., & Perez, F. (1991, September). Design and construction of medium power axial flux induction motors. *In 1991 Fifth International Conference on Electrical Machines and Drives* (Conf. Publ. No. 341) (pp. 260-265). IET.